Polymer Chemistry

ROYAL SOCIETY OF CHEMISTRY

COMMUNICATION

Cite this: *Polym. Chem.*, 2022, **13**, 156

Received 12th September 2021,
Accepted 7th December 2021

DOI: 10.1039/d1py01232k

rsc.li/polymers

Efficient collection of perrhenate anions from water using poly(pyridinium salts) *via* pyrylium mediated transformation†

Xiaorui Li,[a] Liyuan Chai,[a,b] Junyu Ren,[c] Linfeng Jin,[a] Haiying Wang,*[a,b,d] Yiming Li*[e] and Shengqian Ma *[c]

Poly(pyridinium salts) (PPSs) with positive charges on the backbones were designed and synthesized from the transformation of bispyrylium salts. Such materials exhibited good uptake capacity for rhenium capture from water, and excellent selectivity of ReO_4^- from competing anions. Furthermore, the advantages of facile synthesis and large-scale preparation make this material promising for practical use in industry.

Rhenium, as a kind of valuable element usually obtained from the industrial melting wastewater, has been widely used in the field of aerospace and catalysis.[1–3] However, the harsh conditions of wastewater, such as high acidity, excessive competing ions and low original concentration, hamper the capture of rhenium.[4,5] To address this, much effort has been dedicated to the design and synthesis of integrated adsorbents with high stability and excellent selectivity. Recently, cationic polymers have been selected as a promising candidate in industrial application due to their high designability, great thermostability, controllable positive charges and facile ion exchange process for Re capture.[5–11]

In the past decades, poly(pyridinium salts) have received considerable attention due to their extraordinary redox, electronics, electrochromics and liquid-crystalline properties, and have been widely applied in electrochromic display devices, molecular machines, antibacterial agents, supercapacitors and so on.[12–19] In addition, owing to the positive charges on backbones and exchangeable counterions, poly(pyridinium salts) can also be applied for anion pollutant capture in water though ion exchange.[20–22] For instance, polyviologens, as the most famous type of pyridinium-based polymers, were used for oxo-anion removal from water, such as BrO_3^-, CrO_4^{2-}, MnO_4^- and so on.[9,23–25] Recently, porous pyridinium-based polymers also exhibited a record-breaking uptake capacity for TcO_4^-.[6] In order to construct cationic polymers, many approaches have been discovered, such as Zincke reaction, Sonogashira–Hagihara coupling, Menshutkin reaction, imine condensation, free radical polymerization and so on.[26] Another approach to poly(pyridinium salts) is the utilization of pyrylium salts.[18,19] With a positive charge on the oxygen atom, such salts are highly reactive to many nucleophiles to form various heterocyclic compounds, including pyridinium salts.[27] Moreover, by reacting bispyrylium salts with diamines, poly(pyridinium salts) can be easily achieved with advantages of versatile design, cheap reagents, catalyst-free process, and large-scale preparation, which make poly(pyridinium salts) a more promising material for industrial applications.

In this work, a pyridinium-based cationic polymer, named **PPS**, was synthesized through a one-pot condensation reaction. In the structure, functional groups of pyridinium rings play an important part in anion capture. Owing to the positive charges on the backbones, **PPS** exhibited the maximum uptake capacity of 596.0 mg g^{-1} for ReO_4^- capture and good recyclability after running the sorption–desorption process for 5 times. In addition, such material was able to realize deep treatment to 182.5 ppb. Also, this polymer can work in a wide pH range, suggesting the extensive working range of waste water treatment. At the same time, the hydrophobic feature was introduced by the benzene-rich motifs and brought structural rigidity, excellent selectivity and insolubility in water.[28] The high capacity, deep removal treatment, wide working range and excellent selectivity indicated that **PPS** has great potential in the application of ReO_4^- capture from water.

As shown in Scheme 1, **PPS** was successfully synthesized *via* the pyrylium mediated transformation reaction between

[a]*School of Metallurgy and Environment, Central South University, Changsha, Hunan, 410083, China. E-mail: haiyw25@yahoo.com*
[b]*Chinese National Engineering Research Center for Control & Treatment of Heavy Metal Pollution, Changsha, Hunan, 410083, China*
[c]*Department of Chemistry, University of North Texas, Denton, TX, 76201, USA. E-mail: Shengqian.Ma@unt.edu*
[d]*Water Pollution Control Technology Key Lab of Hunan Province, Changsha, Hunan, 410004, China*
[e]*College of Chemistry and Chemical Engineering, Central South University, Changsha, Hunan, 410083, China. E-mail: chemyl@csu.edu.cn*

†Electronic supplementary information (ESI) available. See DOI: 10.1039/d1py01232k

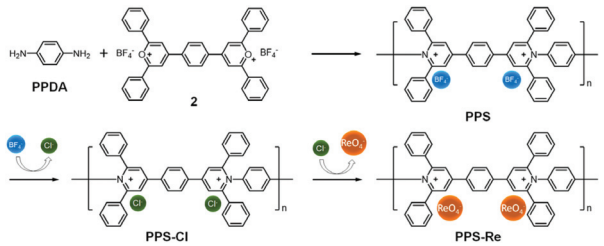

Scheme 1 Synthesis route and anion exchange process of **PPS**.

p-phenylenediamine and bispyrylium salts (compound **2**) in dimethyl sulfoxide (DMSO). The cationic polymer was characterized by multiple techniques to confirm the structure, including SEM, FT-IR, XPS, TGA, PXRD, GPC and ^{13}C NMR. As shown in Fig. 1, the ^{13}C cross-polarization magic-angle spinning (CP/MAS) NMR experiment was first conducted to investigate the structure of **PPS**. As a comparison, model compound **3** (the synthetic route can be found in Scheme S3, ESI†) was synthesized and characterized by ^{13}C NMR spectroscopy to help the peak assignment of **PPS**. Comparing Fig. 1 and Fig. S1† (see the ESI†), the peak at 123.8 ppm observed in Fig. 1 was attributed to C1, C6–C9, and C11 in phenyl rings as well as C4 of pyridinium moieties.[21] Also, the characteristic peaks at 151.5 ppm were assigned to C3 and C5 on pyridinium rings. At the same time, the peak at 134.6 ppm was attributed to C2 and C10 of the phenyl rings.[29] In addition, the integration ratio between three broad peaks was 3 : 2 : 18, which is consistent with the peak assignment. Furthermore, the absence of characteristic peaks at 170.3 ppm (corresponded to C=O$^+$ bond) indicated the disappearance of pyrylium rings in the final product.[30] Also, as evidenced by FT-IR (Fig. 4b), the peak of C=O$^+$ bond stretching at 1660 cm^{-1} was not observed.[30,31] In addition, the characteristic peaks at 1615 cm^{-1} and a broad peak at 1000–1085 cm^{-1} were attributed to the aromatic rings and BF_4^- counterions, respectively.[19,21] This material exhibited a rough surface (as confirmed by the SEM image in Fig. 2a), and its amorphous nature is shown in the PXRD pattern (see Fig. S2 in ESI†). According to the previous reports,[32] with smaller ionic radius (Cl^- as 0.172 nm and BF_4^- as 0.218 nm), Cl^- may lead to a better performance for ReO_4^- removal.[6] However, the monomer pyrylium salt has not been synthesized from HCl directly; BF_4^- was replaced with Cl^- as the counteranion by soaking **PPS** in a sodium chloride solution three times to obtain **PPS-Cl**. As shown in Fig. 2b, thermogravimetric analysis (TGA) under argon atmosphere was conducted to study the thermal stability of **PPS-Cl**. The result revealed that the material was stable up to 330 °C, and the weight loss detected in the temperature range between 550 °C and 650 °C can be attributed to decomposed aromatic rings.[33] It is worth noting that this material retains more than 55% weight at 1000 °C. Meanwhile, GPC was performed and the result showed that the number-average molecular weight and polydispersity of **PPS-Cl** were 19 618 and 1.57, respectively (shown in Table S1 in the ESI†).

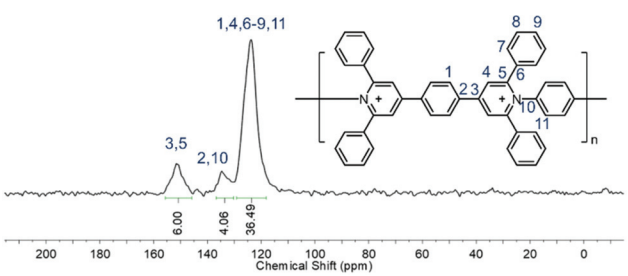

Fig. 1 CP/MAS ^{13}C NMR spectrum of **PPS**.

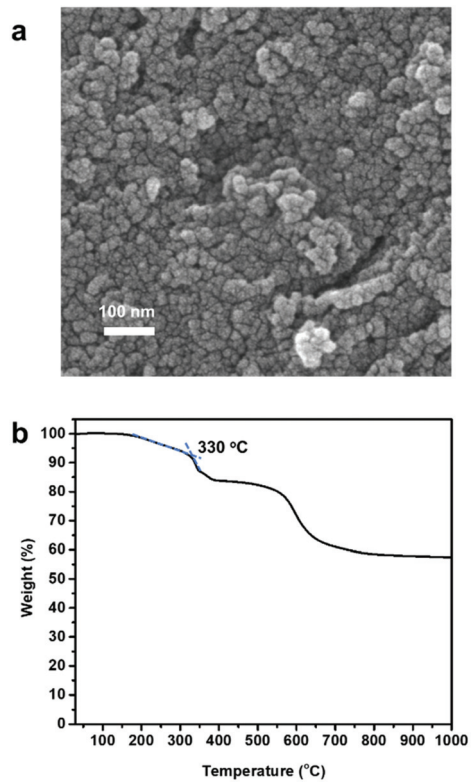

Fig. 2 (a) SEM image of **PPS**, scale bar = 100 nm. (b) TGA of **PPS-Cl** under an Ar atmosphere.

To further investigate the sorption behavior of **PPS**, sorption isotherms and sorption kinetics were first evaluated. The sorption isotherms of **PPS-Cl** were obtained in the range from 10 to 500 ppm for the study of sorption thermodynamics behavior. According to the experimental data, the maximum sorption capacity is 596.0 mg g^{-1} (see Table S2, ESI†), which was lower than the theoretical maximum sorption capacity (731.3 mg g^{-1}) based on the assumed complete exchange process. We speculate that not all of the ion exchange positions were exposed due to the non-porous structure (based on the BET result). On the other hand, the XPS result revealed that not all of the pyrylium rings transferred into pyridinium rings with positive charges (Fig. 4d). Comparing to the Freundlich isotherm model (see Fig. S3, ESI†), the Langmuir

isotherm model showed a higher correlation coefficient (R^2 > 0.99) as shown in Fig. 3a.

Furthermore, the calculated maximum capacity towards ReO_4^- based on the Langmuir isotherm curve of 543.48 mg g^{-1} (see Table S3, ESI†) was slightly lower than the experimental maximum data. At low concentrations (such as 8.5 ppm), **PPS-Cl** still showed excellent ion-exchange ability, and the removal percentage of 97.8% was obtained with an equilibrium concentration in the solution of 182.5 ppb (measured by ICP-MS). Besides, in order to evaluate the sorption kinetics, the equilibrium time was further investigated. The mixture was collected and separated at different time intervals followed by ICP-OES analysis. As shown in Fig. 3b, **PPS-Cl** reached the sorption equilibrium in 150 min (the removal percentage was over 99.4%) and pseudo-second-order models (inset of Fig. 3b) can better describe for sorption kinetics with a high correlation coefficient (R^2 > 0.99, see Table S4, ESI†) than pseudo-first-order models (Fig. S4†).

In order to evaluate the selectivity of **PPS-Cl** for wastewater treatment, SO_4^{2-} was chosen as the competing counterion of ReO_4^-. From the previous report, an extremely high molar ratio between SO_4^{2-} and ReO_4^- (about 4600 : 1) was found in the copper leach solution from the copper smelting plant. Thus, a series of concentrations of SO_4^{2-} was selected to study the sorption selectivity. As shown in Fig. 3c, when the molar ratio of SO_4^{2-} was 10 times and 100 times in excess, the sorption efficiency remained as high as 98.0% and 98.2%, respectively. Surprisingly, even when the molar ratio reaches 5000 : 1, **PPS-Cl** was capable of removing 89.5% of ReO_4^-. Such a feature showed the preference for ReO_4^- capture over excess SO_4^{2-} as competing ions. Also, as shown in Table S5 (ESI†), **PPS-Cl** exhibited superior selectivity between ReO_4^- and SO_4^{2-} among various cationic materials. Based on the HSAB principle, we speculate that the high selectivity can be probably attributed to the charge delocalization of the conjugated benzene-rich structure, which possesses a low positive charge density and has higher affinity for anions with low negative charge densities, such as ReO_4^-.[5,6,34]

Furthermore, the recyclability and pH effect of the material were studied. In Fig. 3d, the recyclability of **PPS-Cl** was evaluated in five cycles of the sorption–regeneration process with 1 M HCl solution. According to the result, the removal percentage was almost unchanged after 5 cycles, which showed an excellent recycling performance. The pH effect on the sorption performance was observed in the pH range from 1 to 12. In Fig. S5 (see ESI),† the removal rate of ReO_4^- of 93.3% at pH 8 was the highest point. Impressively, at pH 1.7 (this value was near the pH value of actual industrial wastewater), the removal percentage of 69.5% was observed even when the molar ratio between Cl^- and ReO_4^- reached 47 : 1 at this time. The zeta potential of **PPS-Cl** in the pH range of 1–13 was obtained to investigate the mechanism of the high adsorption performance in a wide pH range.[35,36] The result in Fig. S6† shows that **PPS-Cl** possessed positive values with pH below 12 and

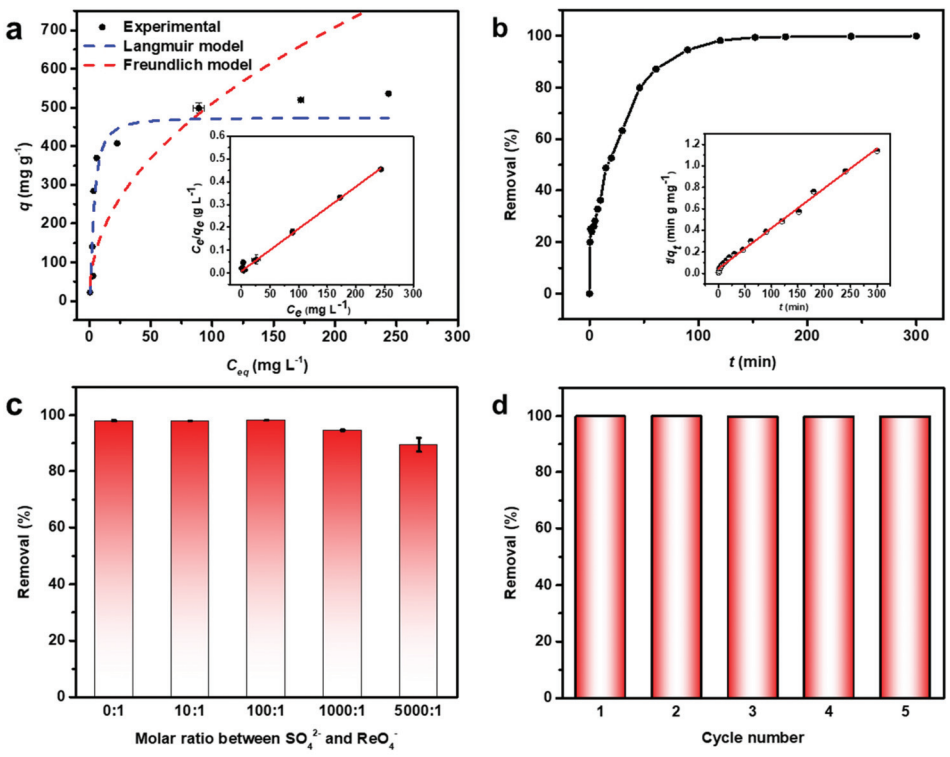

Fig. 3 (a) Sorption isotherm of **PPS-Cl** for ReO_4^- capture, inset shows the fitting curve based on the Langmuir model. (b) Sorption kinetics of **PPS-Cl**, inset shows the fitting curve based on the pseudo-second-order model. (c) Effect of competing SO_4^{2-} anions on the anion-exchange of ReO_4^- by **PPS-Cl**. (d) Reversibility of **PPS-Cl** for collecting ReO_4^-.

negative values with pH higher than 13. As expected, the zeta potential showed high positive values from acidic to weak basic conditions. To further study the removal performance of **PPS-Cl**, simulated industrial water was prepared according to the chemical composition of copper leach solution (see ESI†). Surprisingly, the removal rate of **PPS-Cl** can still reach 94%. All the results demonstrated that **PPS-Cl** is a promising material for industrial wastewater treatment.

The mechanism of the anion-exchange process was investigated by SEM-EDS mapping, FT-IR, Raman spectroscopy and X-ray photoelectron spectroscopy (XPS) analysis. In the FT-IR spectra (Fig. 4b), the characteristic peak at 902 cm^{-1} was shown after the anion-exchange process, which was ascribed to the Re–O stretching mode. In addition, from the Raman spectra (Fig. 4c), the peaks at 965 cm^{-1} and 333 cm^{-1} for ReO_4^- ($NaReO_4$ as reference),[37,38] indicated the successful Re capture by **PPS-Cl**. As confirmed by the XPS survey spectrum of **PPS-Re** (shown in Fig. 4d), the peaks of Re 4p, Re 4d and Re 4f can be observed obviously by comparison to the spectrum of **PPS-Cl**. These results indicated that ReO_4^- as a counterion existed on the surface of the cationic materials after the process of anion exchange. To further study the behavior between the counterion and cationic skeleton, the N 1s (in Fig. 4e) and Re 4f core-level spectra (in Fig. S7, ESI†) were analyzed. After the process of anion exchange, the binding energies of cationic N atoms in the pyridinium ring (N^+) and residual $-NH_2$ and –NH of oligomers at the end group increased from 401.7 eV and 399.7 eV for **PPS-Cl** to 401.8 eV and 399.8 eV for **PPS-Re**.[21] In addition, the binding energies of Re $4f_{5/2}$ and Re $4f_{7/2}$ decreased from 48.4 eV and 46.0 eV for $NaReO_4$ to 47.9 eV and 45.5 eV for **PPS-Re** according to the previous report.[4] This indicated that electrostatic attraction may exist between the cationic skeleton and ReO_4^-. From Fig. 4a, the process of anion exchange can be observed directly based on the SEM-EDS mapping images, and interestingly, the anion exchange process between Cl^- and ReO_4^- was complete. From SEM images in Fig. S8,† the anion exchange process is found to be mild to maintain the morphology.

In conclusion, **PPS-Cl**, representing a cationic pyridinium-based polymer, was designed and synthesized by reacting bis-pyrylium salts with diamines. The advantages of facile synthesis process and large-scale preparation make **PPS-Cl** possible for actual industrial application. At the same time, probably the benzene-rich structure endowed such a material with excellent selectivity, which is a key criterion in waste water treatment.

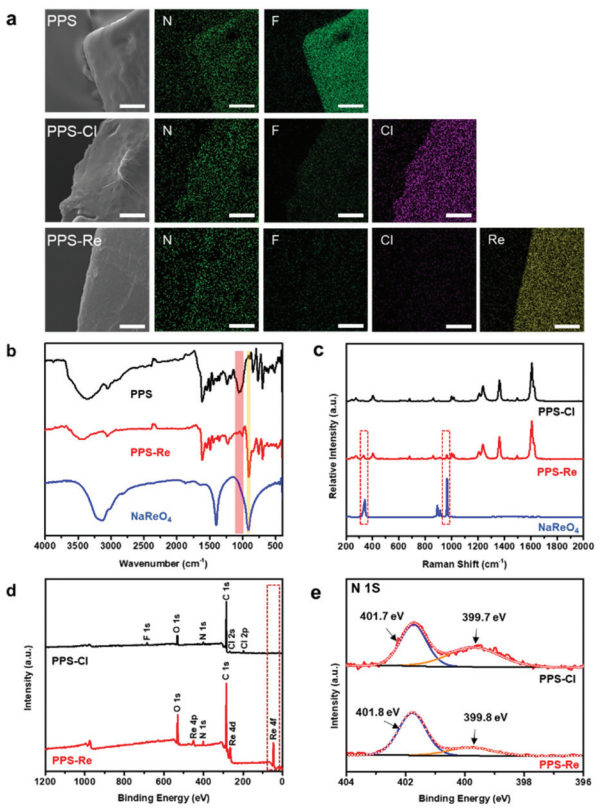

Fig. 4 (a) SEM-EDS mapping of **PPS**, **PPS-Cl**, and **PPS-Re**, indicative of the anion-exchange process. (b) FT-IR spectra of **PPS** before and after anion-exchange with ReO_4^- and $NaReO_4$. Characteristics peaks occurring at 1033 cm^{-1} (red band) and 902 cm^{-1} (yellow band) corresponded to counterion BF_4^- and ReO_4^-, respectively. (c) Raman spectra of **PPS-Cl**, **PPS-Re** and $NaReO_4$. (d) XPS survey spectra of **PPS-Cl** and **PPS-Re**. (e) N 1s core-level spectra of **PPS-Cl** and **PPS-Re**.

Conflicts of interest

There are no conflicts to declare.

Acknowledgements

This work was supported by the National Key R&D Program of China (2018YFC1802204 and 2020YFC1909200), National Natural Science Fund of China for Distinguished Young Scholars (51825403), Innovative Research and Development Institute of Guangdong (2018B090902009) and China Scholarship Council (CSC) (201706370186). Partial support from the U.S. National Science Foundation CBET-1706025 and the Robert A. Welch Foundation (B-0027) is also acknowledged (SM).

References

1 B. Zhang, H.-Z. Liu, W. Wang, Z.-G. Gao and Y.-H. Cao, *Hydrometallurgy*, 2017, **173**, 50–56.
2 H. S. Kim, J. S. Park, S. Y. Seo, T. Tran and M. J. Kim, *Hydrometallurgy*, 2015, **156**, 158–164.
3 D. Bernhardt and J. F. Reilly, *Mineral Commodity Summaries 2019*, U.S. Geological Survey, Reston, VA, 2019.
4 X. Li, Y. Li, H. Wang, Z. Niu, Y. He, L. Jin, M. Wu, H. Wang, L. Chai, A. M. Al-Enizi, A. Nafady, S. F. Shaikh and S. Ma, *Small*, 2021, **17**, 2007994.
5 J. Li, X. Dai, L. Zhu, C. Xu, D. Zhang, M. A. Silver, P. Li, L. H. Chen, Y. Z. Li, D. W. Zuo, H. Zhang, C. L. Xiao,

J. Chen, J. Diwu, O. K. Farha, T. E. Albrecht-Schmitt, Z. F. Chai and S. A. Wang, *Nat. Commun.*, 2018, **9**, 3007.
6 Q. Sun, L. Zhu, B. Aguila, P. K. Thallapally, C. Xu, J. Chen, S. Wang, D. Rogers and S. Ma, *Nat. Commun.*, 2019, **10**, 1646.
7 J. Shen, W. Chai, K. X. Wang and F. Zhang, *ACS Appl. Mater. Interfaces*, 2017, **9**, 22440–22448.
8 Z. W. Liu and B. H. Han, *Environ. Sci. Technol.*, 2020, **54**, 216–224.
9 M. Ding, L. Chen, Y. Xu, B. Chen, J. Ding, R. Wu, C. Huang, Y. He, Y. Jin and C. Xia, *Chem. Eng. J.*, 2020, **380**, 122581.
10 J. Li, L. Chen, N. Shen, R. Xie, M. V. Sheridan, X. Chen, D. Sheng, D. Zhang, Z. Chai and S. Wang, *Sci. China: Chem.*, 2021, **64**, 1251–1260.
11 Y. Song, T. Sun, Q. Chen and X. Shen, *Acta Sci. Nat. Univ. Pekin.*, 2017, **53**, 810–816.
12 J. Ding, C. Zheng, L. Wang, C. Lu, B. Zhang, Y. Chen, M. Li, G. Zhai and X. Zhuang, *J. Mater. Chem. A*, 2019, **7**, 23337–23360.
13 F. Y. Lin, S. Z. D. Cheng and F. W. Harris, *Polymer*, 2002, **43**, 3421–3430.
14 P. K. Bhowmik, S. Kamatam, H. Han and A. K. Nedeltchev, *Polymer*, 2008, **49**, 1748–1760.
15 T. S. Jo, H. Han, L. Ma and P. K. Bhowmik, *Polym. Chem.*, 2011, **2**, 1953–1955.
16 A. K. Nedeltchev, H. Han and P. K. Bhowmik, *Polym. Chem.*, 2010, **1**, 908–915.
17 J. Sun, Y. Lu, L. Wang, D. Cheng, Y. Sun and X. Zeng, *Polym. Chem.*, 2013, **4**, 4045–4051.
18 S. A. X. Huang, K. C. Chuang, S. Z. D. Cheng and F. W. Harris, *Polymer*, 2000, **41**, 5001–5009.
19 F. W. Harris, K. C. Chuang, S. A. X. Huang, J. J. Janimak and S. Z. D. Cheng, *Polymer*, 1994, **35**, 4940–4948.
20 J. Zu, M. Ye, P. Wang, F. Tang and L. He, *RSC Adv.*, 2016, **6**, 18868–18873.
21 S.-Y. Zhang, W.-T. Gong, W.-D. Qu, X.-R. Deng, K.-X. Dong, S.-G. Zhang and G.-L. Ning, *Chin. J. Polym. Sci.*, 2020, **38**, 958–964.
22 T. Sata, *J. Membr. Sci.*, 1996, **118**, 121–126.
23 T. Skorjanc, D. Shetty, F. Gándara, L. Ali, J. Raya, G. Das, M. A. Olson and A. Trabolsi, *Chem. Sci.*, 2020, **11**, 845–850.
24 P. Samanta, P. Chandra, S. Dutta, A. Desai and S. K. Ghosh, *Chem. Sci.*, 2018, **9**, 7874–7881.
25 L. He, S. Liu, L. Chen, X. Dai, J. Li, M. Zhang, F. Ma, C. Zhang, Z. Yang, R. Zhou, Z. Chai and S. Wang, *Chem. Sci.*, 2019, **10**, 4293–4305.
26 T. Skorjanc, D. Shetty, M. A. Olson and A. Trabolsi, *ACS Appl. Mater. Interfaces*, 2019, **11**, 6705–6716.
27 Y. Li, H. Wang and X. Li, *Chem. Sci.*, 2020, **11**, 12249–12268.
28 X. Sun, Y.-K. Yang and F. Lu, *Macromolecules*, 1998, **31**, 4291–4296.
29 J. Lin, S. Bi, Z. Fan, Z. Fu, Z. Meng, Z. Hou and F. Zhang, *Polym. Chem.*, 2021, **12**, 1661–1667.
30 Z. Yang, H. Chen, B. Li, W. Guo, K. Jie, Y. Sun, D. E. Jiang, I. Popovs and S. Dai, *Angew. Chem., Int. Ed.*, 2019, **58**, 13763–13767.
31 S. Che, Z. Yang, I. Popovs, H. Luo, Y. Luo, W. Guo, H. Chen, T. Wang, K. Jie, C. Wang and S. Dai, *Chem. Commun.*, 2019, **55**, 13450–13453.
32 L. Yang, D. Wu, J. Tang, Y. Hao, J. Wang, X. Zhao and P. Yang, *Chem. Phys. Lett.*, 2020, **754**, 137638.
33 Y. Lu, C. Xiao, Z. Yu, X. Zeng, Y. Ren and C. Li, *J. Mater. Chem.*, 2009, **19**, 8796–8802.
34 R. G. Pearson, *J. Am. Chem. Soc.*, 1963, **85**, 3533–3539.
35 Y. Xie, J. Lin, H. Lin, Y. Jiang, J. Liang, H. Wang, S. Tu and J. Li, *J. Hazard. Mater.*, 2020, **392**, 122496.
36 H. Wang, H. Deng, Y. He, L. Huang, D. Wei, T. Hao, S. Wang, L. Jin and L. Zhang, *Chem. Eng. J.*, 2020, **396**, 125249.
37 A. Thevenet, C. Marie, C. Tamain, V. Amendola, A. Miljkovic, D. Guillaumont, N. Boubals and P. Guilbaud, *Dalton Trans.*, 2020, **49**, 1446–1455.
38 B. Zhang, S. Lwin, S. Xiang, A. I. Frenkel and I. E. Wachs, *ACS Catal.*, 2021, **11**, 2412–2421.

